

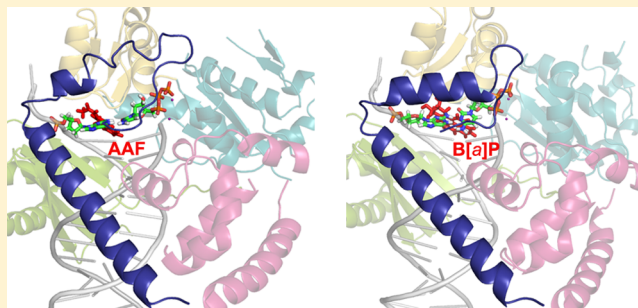
# Structural and Dynamic Characterization of Polymerase $\kappa$ 's Minor Groove Lesion Processing Reveals How Adduct Topology Impacts Fidelity

Lee Lior-Hoffmann,<sup>†</sup> Shuang Ding,<sup>†</sup> Nicholas E. Geacintov,<sup>‡</sup> Yingkai Zhang,<sup>‡</sup> and Suse Broyde<sup>\*,†</sup>

<sup>†</sup>Department of Biology and <sup>‡</sup>Department of Chemistry, New York University, 100 Washington Square East, New York, New York 10003, United States

## Supporting Information

**ABSTRACT:** DNA lesion bypass polymerases process different lesions with varying fidelities, but the structural, dynamic, and mechanistic origins of this phenomenon remain poorly understood. Human DNA polymerase  $\kappa$  (Pol $\kappa$ ), a member of the Y family of lesion bypass polymerases, is specialized to bypass bulky DNA minor groove lesions in a predominantly error-free manner, by housing them in its unique gap. We have investigated the role of the unique Pol $\kappa$  gap and N-clasp structural features in the fidelity of minor groove lesion processing with extensive molecular modeling and molecular dynamics simulations to pinpoint their functioning in lesion bypass. Here we consider the  $N^2$ -dG covalent adduct derived from the carcinogenic aromatic amine, 2-acetylaminofluorene (dG- $N^2$ -AAF), that is produced via the combustion of kerosene and diesel fuel. Our simulations reveal how the spacious gap directionally accommodates the lesion aromatic ring system as it transits through the stages of incorporation of the predominant correct partner dCTP opposite the damaged guanine, with preservation of local active site organization for nucleotidyl transfer. Furthermore, flexibility in Pol $\kappa$ 's N-clasp facilitates the significant misincorporation of dTTP opposite dG- $N^2$ -AAF via wobble pairing. Notably, we show that N-clasp flexibility depends on lesion topology, being markedly reduced in the case of the benzo[*a*]pyrene-derived major adduct to  $N^2$ -dG, whose bypass by Pol $\kappa$  is nearly error-free. Thus, our studies reveal how Pol $\kappa$ 's unique structural and dynamic properties can regulate its bypass fidelity of polycyclic aromatic lesions and how the fidelity is impacted by lesion structures.



High-fidelity DNA polymerases (Pol) are usually blocked by bulky DNA lesions.<sup>1,2</sup> They can be replaced for local translesion synthesis to bypass the distorting DNA damage by one or more bypass polymerases, followed by restoration of the processive and faithful replicative machinery.<sup>3–6</sup> Each of the four human Y family bypass polymerases has unique structural and lesion bypass properties while also possessing common features.<sup>5,7</sup> Human DNA Pol $\kappa$  is similar to other Y family lesion bypass polymerases.<sup>3</sup> It has fingers, palm, and thumb subdomains that comprise the conserved catalytic core, and the DNA substrate is located between the thumb and the little finger or polymerase-associated domain (PAD).<sup>8</sup> In Pol $\kappa$ , there is a uniquely large structural gap on the minor groove side that separates the catalytic core and the little finger, and a unique N-terminal extension (N-clasp) on the DNA major groove side that holds the little finger and the palm/fingers of the catalytic core together (Figure 1A). The functional role of this gap and the N-clasp in lesion bypass by Pol $\kappa$  has attracted considerable interest,<sup>9–11</sup> because Pol $\kappa$  bypasses minor groove bulky DNA lesions that are linked to the amino group of guanine with predominant incorporation of the correct nucleotide dCTP; however, some mutagenic outcome that varies among different lesions is observed.<sup>12–20</sup> Furthermore, adducts that bind to

adenine  $N^6$  or guanine C8 on the major groove side are mainly blocking or more mutagenic.<sup>12,17,21–26</sup>

At present, the structural and dynamic origins of the various outcomes in lesion processing by DNA Pol $\kappa$  are poorly understood. The size and shape of bulky polycyclic aromatic DNA lesions, their site of linkage to different bases, and their stereochemical properties determine their handling by lesion bypass DNA polymerases<sup>12,17,21–24</sup> and other macromolecular machines, such as DNA repair enzymes.<sup>27</sup> Our understanding of the relationships between lesion and polymerase architectures and functions is limited. However, this knowledge is crucially needed to identify the molecular mechanisms underlying lesion-induced mutagenesis. In earlier work, we have shown that the major adduct derived from the environmental procarcinogen benzo[*a*]pyrene (B[*a*]P), (10S)-(+)-trans-anti-B[*a*]P- $N^2$ -dG (dG- $N^2$ -B[*a*]P),<sup>28</sup> is easily accommodated on the minor groove side of the damaged template in Pol $\kappa$  while the (10S)-(+)-trans-anti-B[*a*]P- $N^6$ -dA adduct on the major groove side is sterically constrained by the

Received: June 26, 2014

Revised: August 14, 2014

Published: August 19, 2014

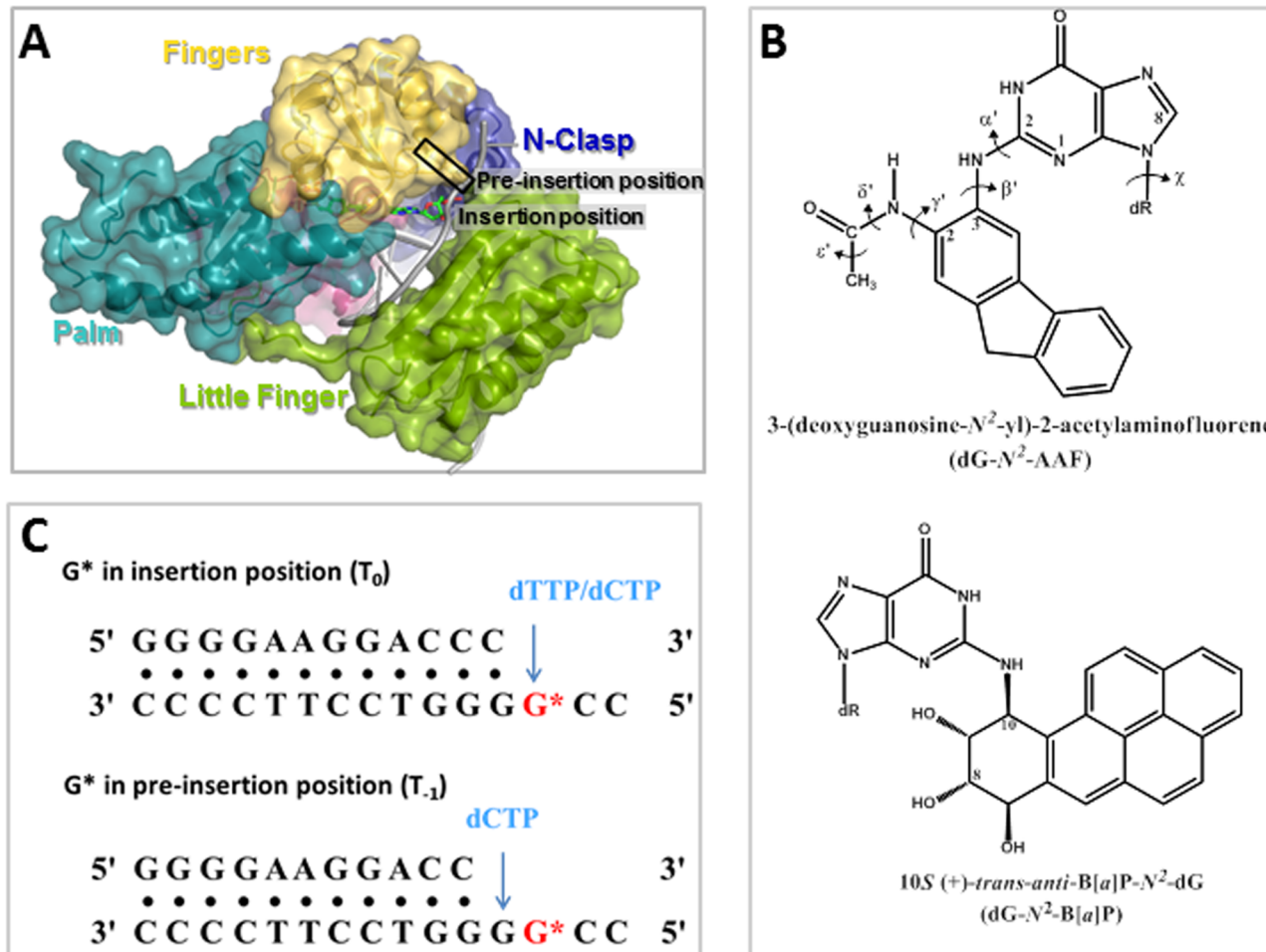


**Figure 1.** Structures and sequences investigated. (A) Ternary crystal structure of Polk (PDB entry 2OH2).<sup>8</sup> The nucleotide at the preinsertion position is hidden behind the fingers domain, and its location is designated with a black frame. (B) Structures of the dG- $N^2$ -AAF and dG- $N^2$ -B[a]P adducts. Torsion angles for dG- $N^2$ -AAF are defined as follows:  $\chi$  for O4' (dR)-C1' (dR)-N9-C4 (dR is deoxyribose),  $\alpha'$  for N1-C2- $N^2$ -C3(AAF),  $\beta'$  for C2- $N^2$ -C3(AAF)-C2(AAF),  $\gamma'$  for C3(AAF)-C2(AAF)-N(AAF)-C(AAF),  $\delta'$  for C2(AAF)-N(AAF)-C(AAF)-Cm(AAF), and  $\epsilon'$  for N(AAF)-C(AAF)-Cm(AAF)-Hm(AAF) (m denotes a methyl group). For the dG- $N^2$ -B[a]P adduct, the ring containing the OH groups is termed the benzylic ring. (C) Base sequences of the preinsertion and insertion models. The incoming nucleotide dNTP is colored blue. G\* denotes the damaged guanine.

Polk N-clasp,<sup>10,11</sup> explaining their respective observed bypass and blocking properties in primer extension studies.<sup>17</sup>

To pursue the goal of investigating impacts of lesion topology and stereochemistry on the fidelity of lesion processing by Polk, we investigate an adduct derived from the carcinogenic aromatic amine 2-acetylaminofluorene (AAF), 3-(deoxyguanosin- $N^2$ -yl)-2-acetylaminofluorene (dG- $N^2$ -AAF or dG\*) (Figure 1B). This lesion shares its  $N^2$ -dG linkage site with dG- $N^2$ -B[a]P but is less bulky with three rather than four aromatic rings and no chiral center at the linkage site. Moreover, it is planar, while dG- $N^2$ -B[a]P contains the nonplanar and OH-bearing benzylic ring (Figure 1B). However, the AAF adduct contains the bulky acetyl group. The AAF lesion can be produced by exposure to the environmental contaminant 2-nitrofluorene, a major byproduct of kerosene and diesel combustion.<sup>29,30</sup> The adduct is housed in the B-DNA minor groove in solution where it increases the thermal and thermodynamic stability of the B-DNA duplex.<sup>31</sup> It is persistent in mammalian tissues,<sup>32–34</sup> consistent with its thermodynamic lesion-induced DNA duplex stabilization, which is associated with nucleotide excision repair resistance.<sup>27,35</sup> However, protection against transcriptional errors by

this lesion via transcription-coupled nucleotide excision repair<sup>36–38</sup> has recently been demonstrated,<sup>39</sup> indicating that its persistence results from resistance to global genomic nucleotide excision repair.<sup>40,41</sup> Primer extension studies show that Polk bypasses the dG- $N^2$ -AAF lesion with predominant incorporation of dCTP but also with significant misincorporation of dTTP *in vitro*.<sup>18</sup> The lesion's persistence and its mutagenicity in mammalian cells suggest that this minor AAF-derived adduct can readily survive to replication and cause cancer-initiating mutations; in simian kidney (COS-7) cells, G → T transversions were the predominant observed targeted mutations, but bypass was mainly error-free.<sup>18</sup>

In this study, we have characterized structural and dynamic factors governing the fidelity of processing of dG- $N^2$  minor groove adducts by Polk. With extensive molecular modeling and molecular dynamics simulations, we have gained a detailed molecular and dynamic characterization of dG- $N^2$ -AAF lesion bypass through stages of the replicative process as the lesion transits from the preinsertion to the insertion position and then to the chemical transition state for the nucleotidyl transfer reaction.<sup>10</sup> We provide a new understanding of Polk's structural architecture for bypass of minor groove lesions by revealing

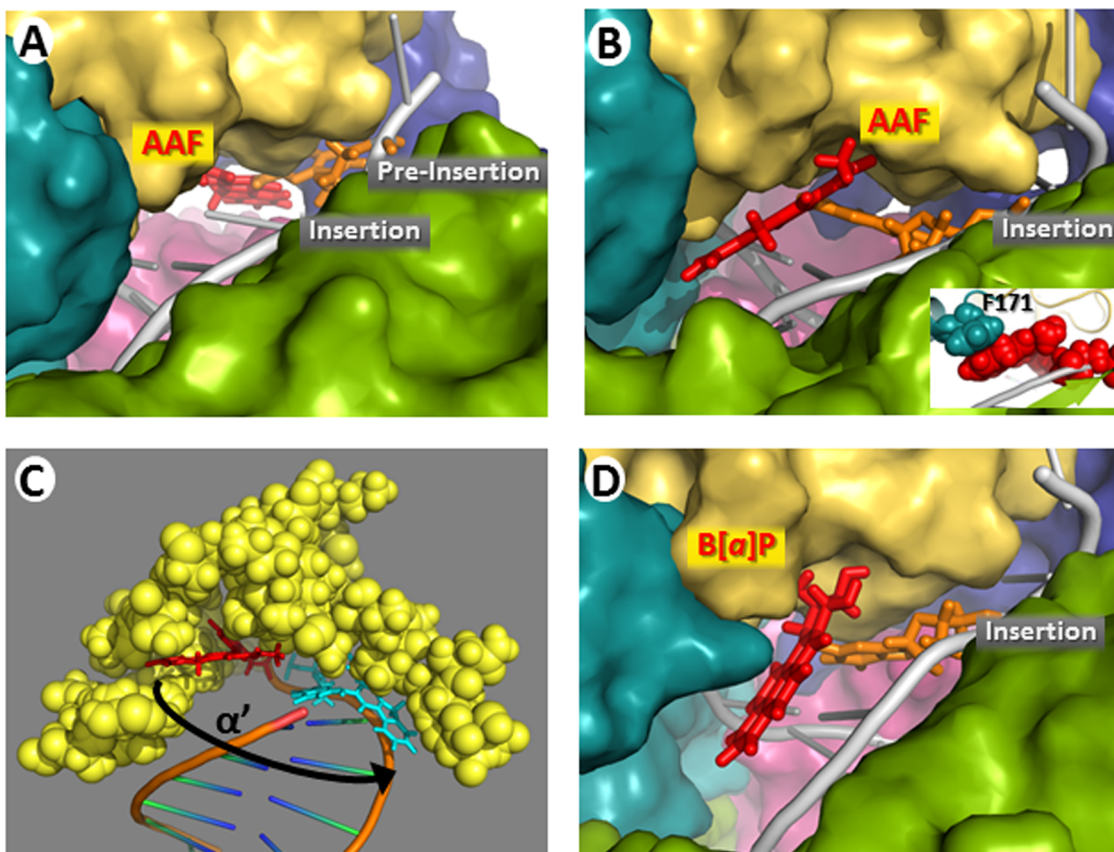


**Figure 2.** Lesion structures in the Polk gap at preinsertion and insertion positions. Polk containing the dG-N<sup>2</sup>-AAF adduct (A) in the preinsertion position and (B) in the insertion position opposite dCTP. dG-N<sup>2</sup>-AAF in the insertion site exhibits favorable stacking interactions with Phe171 as shown in the inset. (C) As the damaged base translocates through the gap in Polk from the preinsertion site (dG-N<sup>2</sup>-AAF in red sticks) to the insertion site (dG-N<sup>2</sup>-AAF in cyan sticks), the fluorenyl rings rotate ~180° around the  $\alpha'$  torsion angle (see Movie S1 of the Supporting Information). The part of the protein that comprises the gap region through which translocation occurs is shown as yellow spheres. (D) Polk containing the dG-N<sup>2</sup>-B[a]P adduct in the insertion position. Color scheme for panels A, B, and D: dG-N<sup>2</sup>-AAF and dG-N<sup>2</sup>-B[a]P as red sticks, damaged guanine as orange sticks, N-clasp as a blue surface, thumb domain as a magenta surface, fingers domain as a yellow surface, and DNA template strand as a gray cartoon.

how the flexibility of its N-clasp and its housing of lesions in the minor groove gap are impacted differently by the structurally dissimilar dG-N<sup>2</sup>-AAF and dG-N<sup>2</sup>-B[a]P lesions to yield different balances of mutagenic and nonmutagenic outcomes. Thereby, we show how the fidelity of the human Polk bypass polymerase is regulated by lesion topology.

## METHODS

**Models of Polk with Unmodified DNA.** The ternary crystal structure (PDB entry 2OH2<sup>42</sup>) of Polk<sub>19–526</sub> with DNA and incoming dTTP<sup>8</sup> was the basis for all our prepared enzyme–substrate models. The sequence utilized, shown in Figure 1C, was the same as in the crystal except that it was remodeled in previous work to provide a template G and incoming dCTP; the crystal structure had also been remodeled to create a reaction-ready active site with two Mg<sup>2+</sup> ions,<sup>10</sup> based on a high-resolution crystal structure of a complete DNA polymerase  $\beta$  catalytic complex.<sup>43</sup> With 100 ns MD, we utilized this unmodified ternary complex as a control for the dG-N<sup>2</sup>-AAF simulations.

For simulations involving the pentacovalent phosphorane transition state in the water-mediated and substrate-assisted (WMSA) mechanism (Figure S1 of the Supporting Information), we utilized our previously obtained transition state

structure determined by *ab initio* quantum mechanics/molecular mechanics (QM/MM) simulations.<sup>10</sup>

**Initial Models with the dG-N<sup>2</sup>-AAF Adduct for 100 ns MD Simulations.** We utilized the remodeled, unmodified Polk structure to obtain models of the dG-N<sup>2</sup>-AAF lesion in the preinsertion and insertion positions (Figure 1C). The nuclear magnetic resonance (NMR) solution structure (PDB entry 2GE2<sup>31</sup>) provided initial guidance for modeling of the lesion with minimal collisions. For the very crowded preinsertion site, we could only create a model in which only the fluorenyl ring system fits in the small cavity at the apex of the gap; here the lesion can be housed on the damaged guanine's evolving major groove side. The minor groove side of the evolving duplex was entirely obstructed by the fingers (Figure 1A). Table S1 of the Supporting Information gives linkage site torsion angle values for  $\alpha'$ ,  $\beta'$ ,  $\gamma'$ ,  $\delta'$ ,  $\epsilon'$ , and  $\chi$  (Figure 1B) and Met115 (whose side chain also had to be remodeled) for this initial model for MD.

For the insertion site, we modeled two orientations for the dG-N<sup>2</sup>-AAF adduct. In the NMR solution structure, the fluorenyl ring system is directed 5' along the damaged strand in the minor groove. In addition, computational studies<sup>44</sup> had shown that a 3' orientation was also feasible, and we investigated this orientation, as well. Using the NMR solution structure as a guide, we covalently linked the AAF moiety to the template *anti* G amino group in the unmodified ternary

complex model and adjusted torsion angles  $\alpha'$ ,  $\beta'$ ,  $\gamma'$ ,  $\delta'$ ,  $\epsilon'$ , and  $\chi$  (Figure 1B) to obtain 3'- and 5'-oriented structures; this also required a change in a side chain torsion angle of Phe171. We considered both incoming dCTP and dTTP. Table S1 of the Supporting Information gives linkage site torsion angle values for  $\alpha'$ ,  $\beta'$ ,  $\gamma'$ ,  $\delta'$ ,  $\epsilon'$ ,  $\chi$ , and Phe171 for these initial models for MD. For dCTP, we maintained Watson–Crick pairing as in the unmodified model.<sup>10</sup> For the mismatched dTTP, we created a wobble pair with dG\*:dTTP paired with N1H1(G)…O2(T) and O6(G)…N3H3(T) hydrogen bonds (Figure S2 of the Supporting Information). For the study of the transition state, we remodeled our previously obtained transition state structure determined by a QM/MM–MD investigation<sup>10</sup> to contain the lesion in its preferred 3' orientation in the ternary complex before reaction (see Results). The unmodified transition state structure was used for a control simulation. All initial models were prepared using INSIGHT II 2005 (Accelrys Software, Inc.).

**Force Fields and Molecular Dynamics.** MD simulations were conducted using the PMEMD module of the AMBER 11 simulation package<sup>45</sup> with Amber99SB<sup>46–48</sup> and GAFF<sup>49</sup> force fields and the TIP3P water model.<sup>50</sup> A new AMBER-compatible force field set was developed for the dG-N<sup>2</sup>-AAF adduct and is given in Table S2 of the Supporting Information. For dCTP and dTTP, we utilized previously calculated parameters.<sup>51</sup> For the transition state models, we utilized our previously developed parameters<sup>10</sup> for dCTP as the incorporated nucleotide, and we developed a new parameter set for the transition state model for dTTP as the incorporated nucleotide (Table S2 of the Supporting Information).

For each model, a 100 ns MD simulation was performed after initial equilibration. The last snapshot of the simulation was used to illustrate the structures, except where indicated. All analyzed properties are ensemble averages over the entire 100 ns MD simulations. Trajectory analyses were conducted with the P traj and Carnal packages of Amber 11. Full details of the MD and force field protocols are given in the Supporting Information. PyMOL<sup>52</sup> was employed to make molecular images and the movies.

## RESULTS

In Polk, we have investigated the dG-N<sup>2</sup>-AAF adduct in three positions: (1) the preinsertion site to determine how feasible it is for the adduct to translocate from the preinsertion site to the insertion site, (2) the insertion site opposite dCTP and dTTP (Figure S2 of the Supporting Information), and (3) the pentacovalent phosphorane transition state, which is formed during the nucleotidyl transfer reaction in the WMSA mechanism previously determined by QM/MM–MD calculations for Polk (Figure S1 of the Supporting Information).<sup>10,53</sup> We have used molecular modeling and molecular dynamics simulations (detailed in Methods) to gain an understanding on a molecular and dynamic level of the cycle of events in the Polk active site and thereby obtain insights into the fidelity of Polk's processing of minor groove polycyclic aromatic lesions.

**The Adduct in the Preinsertion Site Can Be Housed in the Crevice at the Apex of the Gap.** Our modeling for dG-N<sup>2</sup>-AAF in the preinsertion site showed that the adduct can fit only on the major groove side pointing in the 5' direction of the damaged strand in a crevice at the apex of the gap, while the minor groove side is crowded by the fingers (Figure 1A). This positioning is preserved following 100 ns MD as shown in Figure 2A. Ensemble average torsion angle values for  $\alpha'$ ,  $\beta'$ ,  $\gamma'$ ,

$\delta'$ ,  $\epsilon'$ , and  $\chi$  (Figure 1B) and Met115 are listed in Table S1 of the Supporting Information. The glycosidic torsion of the damaged guanine is very dynamic but remains largely in the overall *anti* domain (Figure S2 of the Supporting Information)

**In the Insertion Site, the Lesion Is Housed in the Polk Gap Directed 3' along the Modified Strand toward the Duplex Region.** From our modeling efforts, we obtained two initial conformations for MD simulations that comfortably accommodate the fluorenyl rings in the Polk gap, between the fingers and the palm on one side and the little finger on the other side, and with a dCTP partner: (1) with the AAF ring system oriented toward the single-stranded overhang and directed 5' along the modified strand, as in the NMR solution structure in duplex DNA,<sup>31</sup> and (2) with the AAF ring system directed toward the duplex region in a 3' orientation, as predicted computationally.<sup>44</sup> Ensemble average linkage site torsion angle values are summarized in Table S1 of the Supporting Information. The Watson–Crick pairing was retained in the MD simulations of both orientations. Also, the active site is as well organized in the structures containing lesions as in the unmodified control; key properties include maintenance of the octahedral coordination of the Mg<sup>2+</sup> ions, the in-line O3'–P<sub>a</sub> attack distance, maintenance of interactions with key amino acid residues, and preservation of the two water molecules participating in the WMSA mechanism.<sup>10</sup> In this respect, both MD models appear equally feasible. The dG\*:dCTP (dG\* denotes the damaged base) model in the 3' orientation of the fluorenyl rings is illustrated in Figures 2B and 3A, and full details are given in Figure S3 and Table S3 of the Supporting Information. The active site organization of the 5'-

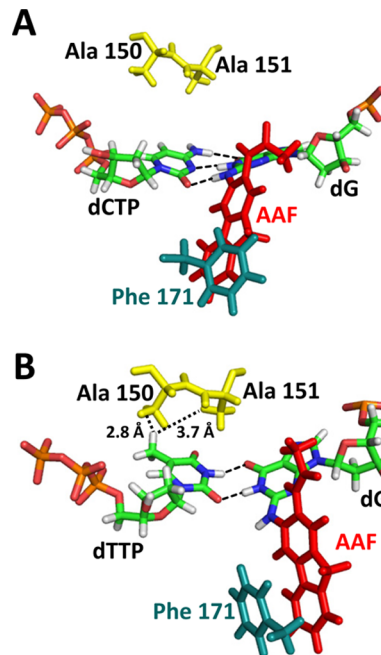


**Figure 3.** Watson–Crick and wobble pairing for dG-N<sup>2</sup>-AAF. (A) dG-N<sup>2</sup>-AAF Watson–Crick pair with dCTP. (B) dG-N<sup>2</sup>-AAF wobble pair with the dTTP mismatch. Methyl groups of Ala150 and Ala151 from the fingers domain have van der Waals interactions with the dTTP methyl group. The shortest distances between methyl hydrogen atoms are given. Dashed lines denote hydrogen bonds, with occupancies all above 95%, given in Table S3 of the Supporting Information. Snapshots at 92 and 86 ns were selected as being representative for panels A and B, respectively.

oriented model is similar (data not shown). However, there are important differences. In the 5'-directed case, the fluorenyl distal aromatic ring is entirely solvent-exposed on one face and steric crowding causes the distortion of the fingers (Figure S4 of the Supporting Information), while in the 3'-directed orientation, the entire aromatic ring system is neatly sandwiched in the gap (Figure 2B). In addition, the 3'-directed orientation has a favorable dynamic stacking interaction with Phe171 that is not present for the 5' case, where the ring system is directed away from Phe171. Figure 2B and Figure S4 of the Supporting Information show the differences in these interactions. For these reasons, the 5' orientation is disfavored.

**The Pentacovalent Transition State Structure Remains Stable with a 3'-Oriented Lesion.** For investigation of the transition state structure in the WMSA mechanism (Figure S1 of the Supporting Information),<sup>10,53</sup> we used the favorable 3' lesion orientation with dCTP to establish whether the pentacovalent phosphorane and the local organization were maintained in the presence of the dG-N<sup>2</sup>-AAF adduct. Our results of the 100 ns MD simulation showed that the transition state structure is well-maintained (Figure 4 and Figure S3 and

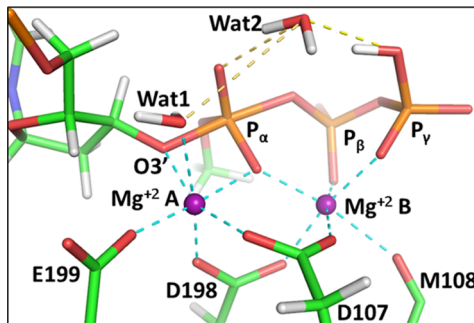


**Figure 4.** Pentacovalent phosphorane transition state with dCTP incorporated into the dC priming nucleotide. Polk's active site at the transition state maintains the octahedral coordination of the two Mg<sup>2+</sup> ions (shown with the blue dashed lines) and the water molecules utilized in the WMSA mechanism<sup>10</sup> to shuttle the proton from the γ-phosphate to the α,β-bridge (yellow dashed lines) as pyrophosphate leaves.

Table S3 of the Supporting Information): the geometry of the pentacovalent phosphorane transition state, the geometry of the protonated γ-phosphate ready to transfer its proton to the α,β-oxygen bridge, hydrogen bonding interactions with amino acids that stabilize the transition state, Mg<sup>2+</sup> ion coordination, and base pairing between the template and the incoming dCTP.

**Wobble Pairing Stabilizes an Incoming dTTP Mismatch.** While incorporation of dCTP opposite dG-N<sup>2</sup>-AAF predominated in the primer extension studies in Polk, a significant amount of dTTP was also misincorporated.<sup>18</sup> To determine how a dG\*:dTTP mismatch is accommodated in the polymerase active site, we created an initial model with *anti*-dG-N<sup>2</sup>-AAF in the favored 3' orientation and wobble paired with incoming dTTP (Figure S2 of the Supporting Information). Following a 100 ns MD simulation, we found that a nicely aligned, well-hydrogen-bonded wobble pair was maintained for the reactant state (Figure 3B), and also for the subsequent 100 ns transition state simulation (Figure S5 of the Supporting Information). The dynamic stacking interaction between Phe171 and the AAF ring system is present as in the case of the Watson–Crick base pair. In addition, an analysis of the

active site region of Polk showed the presence of Ala residues 150 and 151, whose methyl groups have favorable van der Waals interactions with the methyl group of thymine, which seems to aid in stabilizing the incorporation of dTTP (Figure 3B and Figure S5 of the Supporting Information). Both simulations maintained well-organized active sites; details are given in Figure S3 and Table S3 of the Supporting Information. Ensemble average linkage site torsion angle values are listed in Table S1 of the Supporting Information.

### Translocation of the Adduct from the Preinsertion Site to the Insertion Site through the Gap Is Feasible.

Evaluating the MD structures of the preinsertion and insertion sites to consider translocation to the insertion site, we found that the adduct would need to rotate around α' (Figure 1B) as the strand translocates; α' adopts a value of 19.6 ± 12.3° (range of 8.7–30.4°) in the preinsertion site and 150.6 ± 45.0° (range of 98.1–160.9°) in the insertion site opposite dCTP in its 3' favored orientation (Figure S2 and Movie S1 of the Supporting Information). The large standard deviations and ranges indicate opportunities for significant conformational flexibility, particularly in the insertion site. This is seen in Figure 2B, which shows the aromatic ring system housed in the gap and oriented in the 3' direction of the template strand, toward the palm. The gap is sufficiently spacious to allow the bulky adduct on the major groove side in the preinsertion position to translocate to the minor groove side in the insertion position, as shown in Figure 2C and Movie S1 of the Supporting Information.

**MD Simulations Show That the N-Clasp Is Flexible.** We observed flexibility of the N-clasp domain. This dynamic appeared along the MD trajectories of unmodified (Movie S2 of the Supporting Information) and modified (Movies S3 and S4 of the Supporting Information) models, but to a greater extent in the models with the AAF-damaged templates. Of special interest is the region of the tether between αN1 and αN2 that dynamically elongates and shortens because of the unwinding of primarily the αN1 helix. This dynamic allows conformational flexibility in the template strand, which likely facilitates the wobble pairing with dTTP for the dG-N<sup>2</sup>-AAF adduct (Movie S4 of the Supporting Information). However, as discussed below for the dG-N<sup>2</sup>-B[*a*]P adduct, lesion topology significantly impacts this flexibility.

## DISCUSSION

**Lesion Housing in the Minor Groove Gap for Bypass by Polk.** Our modeling and molecular dynamics studies show that the dG-N<sup>2</sup>-AAF lesion is well-accommodated in the Polk gap opposite dCTP. We investigated this minor groove lesion at the insertion site, directed either 5' or 3' along the modified strand in the gap, based on its NMR solution structure<sup>31</sup> and computational modeling studies.<sup>44</sup> However, the 3' orientation fits distinctly better in the gap (Figure 2B and Figure S4 of the Supporting Information). The fluorenyl rings are neatly sandwiched between the fingers/palm and the little finger, forming van der Waals contact with the fingers/palm domains on one face, and are well-protected from solvent. Also, the adduct is well-aligned with the damaged strand, and the distal aromatic ring stacks dynamically with Phe171. In contrast, in the 5' orientation, the fluorenyl rings crowd the fingers domain and deform the gap, and they are not positioned for stacking with Phe171 (Figure S4 of the Supporting Information). Moreover, the distal aromatic ring protrudes from the DNA double helix, extruding from the protein surface, and thus is solvent-exposed. Therefore, the 3'-oriented conformer is clearly

favorable. Furthermore, Watson–Crick pairing and all other hallmarks of the reaction-ready state are preserved, including the water molecules that participate in the WMSA mechanism (Figure S1 of the Supporting Information), which retain positions to permit shuttling of the O<sub>3'</sub> proton to the  $\gamma$ -phosphate. In addition, simulations of the transition state also show the same stability (Figure 4 and Figure S3 and Table S3 of the Supporting Information). Only two Mg<sup>2+</sup> ions<sup>54</sup> are needed to stabilize the transition state in the low-energy reaction path of the WMSA mechanism,<sup>10,53</sup> but recent structural evidence indicates that a third metal ion can aid in charge stabilization as the reaction proceeds in Pol $\eta$  and Pol $\beta$ .<sup>55–57</sup> Future work will provide further insights into the roles of the metal ions in nucleotidyl transfer with various polymerases.

Our models of the preinsertion site containing the dG-N<sup>2</sup>-AAF lesion show that its fluorenyl rings can be well-housed in a crevice of the gap, on the major groove side of the evolving duplex (Figure 2A). Notably, we show that translocation from the preinsertion to the insertion site via rotation of  $\alpha'$  (Figure S2 of the Supporting Information) is unobstructed through the gap between the fingers/palm and little finger domains (Figure 2C and Movie S1 of the Supporting Information). Thus, our results provide structural and dynamic explanations for the observed preferred incorporation of dCTP for this adduct in Polk. Our models suggest that other polycyclic aromatic lesions, such as the dG-N<sup>2</sup>-B[a]P adduct, could be similarly accommodated in the preinsertion site and translocate through the gap to the insertion site.

**dG:dTTP Mismatches Are Facilitated by N-Clasp Flexibility for Stable Wobble Pairing.** Experimental results showed that dTTP is misincorporated to a significant extent opposite dG-N<sup>2</sup>-AAF;<sup>18</sup> our models and MD simulations showed that an anti-dG\*:dTTP wobble pair was well-accommodated at the insertion site with maintenance of waters and reaction-ready geometry, and that the transition state structure was also preserved (Figure S3 and Table S3 of the Supporting Information). We examined the active site region to gain insight into the preference for dTTP over other mismatches and noted a pair of Ala residues positioned so that their methyl groups engaged in favorable van der Waals interactions with the thymine methyl group (Figure 3B). The flexible N-clasp and the favorable interactions with Ala may also play a part in the observed preference of Polk to incorporate dTTP opposite template G above other mismatches<sup>13,18,21</sup> opposite unmodified template dG.

Deletion of a part or the whole N-clasp domain of Polk reduces the polymerase activity.<sup>8</sup> The N-clasp completes the encircled grip around the primer/template pair at the insertion position, and it was suggested that, by inducing conformational changes from disordered to ordered states when binding to DNA, it locks all the domains of Polk around the DNA.<sup>8</sup> Recently, Liu et al.<sup>9</sup> highlighted that the N-clasp is essential for bridging the minor groove gap by forming van der Waals interactions with the little finger, but that it is flexible. Our simulations revealed the flexibility of the N-clasp domain: the region of the tether between  $\alpha$ N1 and  $\alpha$ N2 is of particular interest; it dynamically elongated and shortened because of the unwinding of primarily the  $\alpha$ N1 helix. Moreover, the dynamics appeared along the MD trajectories of all models (Movies S2–S4 of the Supporting Information), but to a greater extent in the models with AAF-damaged templates (Figure 5 and Movies S3 and S4 of the Supporting Information). This dynamics

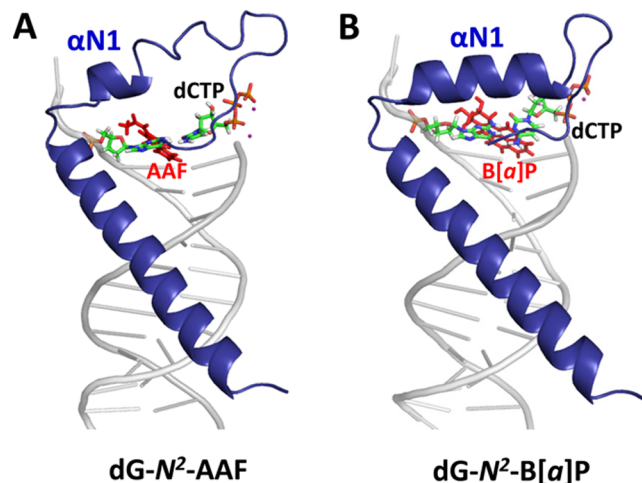


**Figure 5.**  $\alpha$ N1 of the N-clasp domain is more flexible in (A) dG-N<sup>2</sup>-AAF than in (B) dG-N<sup>2</sup>-B[a]P. The most representative structures for  $\alpha$ N1 throughout the 100 ns trajectory are shown.

allows mobility in the template strand, which facilitates the wobble pairing between an incoming dTTP and dG\*, because the N-clasp flexibility permits the template base to position itself optimally for wobble pair geometry.

**Lesion Topology Influences N-Clasp Flexibility, Which Impacts Polk Fidelity.** Polk is also responsible for the near error-free bypass *in vitro*<sup>17,58</sup> of the more bulky minor groove dG-N<sup>2</sup>-B[a]P adduct (Figure 1B).<sup>59</sup> In this case, nucleotide misincorporation is much more rare<sup>17</sup> than for the dG-N<sup>2</sup>-AAF case.<sup>18</sup> Furthermore, Polk appears to be utilized in near error-free bypass of the dG-N<sup>2</sup>-B[a]P minor groove adduct *in vivo* as well,<sup>58,60–62</sup> with the aid of Pol $\zeta$  for extension.<sup>63</sup> Our previous investigations by modeling and MD methods<sup>10,11</sup> have shown that this lesion is housed in Polk like the dG-N<sup>2</sup>-AAF adduct opposite dCTP, with aromatic ring directed 3' along the modified strand, sandwiched in the gap, protected from solvent, aligned with the DNA template strand, and stacked with Phe171. In this lesion, the 5' orientation, seen in the NMR solution structure,<sup>59</sup> appears to be much more unfavorable than for the dG-N<sup>2</sup>-AAF adduct in Polk, because the four bulkier aromatic rings would offer greater steric hindrance to the finger region of the gap. In addition, we have shown that the pentacovalent phosphorane transition state in the WMSA mechanism for the nucleotidyl transfer reaction (Figure S1 of the Supporting Information) is stable when the B[a]P lesion is present.<sup>10</sup> The placement of the B[a]P ring system in the Polk gap is supported by the work of Liu et al.<sup>9</sup> These workers designed mouse Polk variants with a reduced gap size and reported efficient DNA synthesis across from unmodified DNA and blockage by the dG-N<sup>2</sup>-B[a]P adduct, proving the positioning of the B[a]P ring system in the gap. In their models of Polk mutants, the lesion is placed in the gap directed 3' along the template strand, as in our predicted orientation.<sup>10,11</sup>

To explore the flexibility of the N-clasp in the B[a]P lesion, we extended our previous short simulation<sup>11</sup> to 100 ns (Figure 2D) and found that the N-clasp is much less flexible (Movie S5 of the Supporting Information) than for the dG-N<sup>2</sup>-AAF cases (Figure 5). In this trajectory, we observed a hydrogen bond between the dG-N<sup>2</sup>-B[a]P nonplanar benzylic ring C8-OH (Figure 1) and the in-chain carbonyl oxygen of Met135 (Figure 6A and Figure S6 and Movie S6 of the Supporting

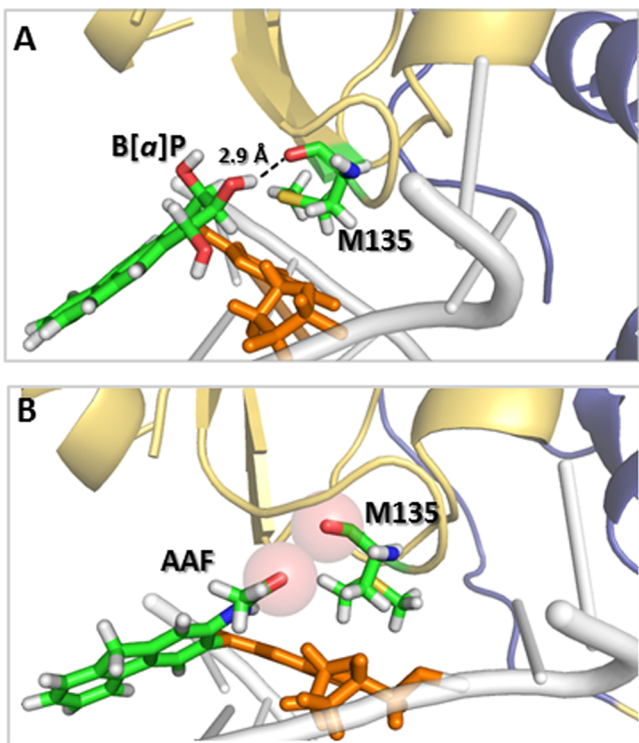


**Figure 6.** Impact of lesions on Met135. (A) The dG-N<sup>2</sup>-B[a]P adduct benzyl ring C8-OH hydrogen bonds with the in-chain carbonyl of Met135. (B) The dG-N<sup>2</sup>-AAF acetyl group carbonyl is repulsive to the in-chain carbonyl of Met135. The B[a]P and AAF moieties and Met135 are colored by atom: C, green; N, blue; O, red; S, yellow; H, white. The protein domains are colored as in Figure 2A.

Information). On the other hand, the acetyl group of the dG-N<sup>2</sup>-AAF adduct is bulky and dynamic, and its carbonyl is repulsive to the carbonyl of Met135 (Figure 6B and Movie S7 of the Supporting Information), leading to a cascade of disturbances between the fingers and the N-clasp via the adjacent Met135. By contrast, the B[a]P hydrogen bond to Met135 provides stability in this region. With the lesser dynamics in the B[a]P case, nucleotide misincorporation through altered hydrogen bonding schemes such as wobble pairing will be less facile.

Taken together, our results provide new structural and dynamic insights into how the spacious Polk gap and flexible N-clasp facilitate bypass of minor groove polycyclic aromatic lesions and show how lesion topology provides structural and dynamic signals that determine the extent of fidelity in bypass by Polk. We determine for the first time how such lesions can be housed in the preinsertion site and translocate through the gap to the insertion site. In this position, we reveal how the distinct features of lesion topology govern the N-clasp's flexibility, which in turn impacts the fidelity of translesion synthesis. Our results show why the dG-N<sup>2</sup>-AAF lesion manifests a significant propensity to misincorporate dTTP through wobble pairing facilitated by N-clasp flexibility, while the dG-N<sup>2</sup>-B[a]P adduct imposes diminished flexibility and is bypassed in a nearly error-free manner by Polk.<sup>17</sup> More broadly, our work points to the lesion dependence of Polk's processing in mutagenic and faithful lesion bypass and hence the degree of protection against mutagenesis by environmental carcinogens that this bypass polymerase can afford.

## ASSOCIATED CONTENT

### Supporting Information

Details of the force field and MD simulation protocol, the water-mediated and substrate-assisted (WMSA) mechanism, anti-dG\* conformation in the preinsertion site and insertion site, maintenance of active site organization along the 100 ns MD simulations, model of dG-N<sup>2</sup>-AAF in the insertion site oriented in the 5' direction of the modified template strand, maintenance of transition state features with dG\*:dTTP wobble pairing, hydrogen bond distance between the dG-N<sup>2</sup>-B[a]P benzylic ring and Met135, torsion angle values in initial models and MD-simulated structures, base pair hydrogen bond occupancies and maintenance of active site organization, force field parameters, and videos showing dG-N<sup>2</sup>-AAF translocation, N-clasp flexibility with the unmodified and modified duplex, and interactions of the adducts with Met135. Note: Movie S1 is the second Supporting Information file listed (bi5007964\_si\_002.avi), followed by Movies S2 to S7 (bi5007964\_si\_003.avi to bi5007964\_si\_008.avi, respectively). This material is available free of charge via the Internet at <http://pubs.acs.org.org>.

## AUTHOR INFORMATION

### Corresponding Author

\*E-mail: broyde@nyu.edu. Telephone: (212) 998-8231. Fax: (212) 995-4015.

### Funding

This work was supported by National Institutes of Health Grants R01-CA-75449 and R01-CA-28038 to S.B., R01-GM079223 to Y.Z., and R01-CA-168469 to N.E.G.

### Notes

The authors declare no competing financial interest.

## ACKNOWLEDGMENTS

In this work, we used the computational resources of the Extreme Science and Engineering Discovery Environment (XSEDE), which is supported by National Science Foundation Grant MCB060037, and the Multipurpose High Performance Computing Resources of New York University (NYU-ITS).

## ABBREVIATIONS

Polk, DNA polymerase  $\kappa$ ; AAF, 2-acetylaminofluorene; dG-N<sup>2</sup>-AAF, 3-(deoxyguanosin-N<sup>2</sup>-yl)-2-acetylaminofluorene; B[a]P, benzo[a]pyrene; dG-N<sup>2</sup>-B[a]P, (1OS)-(+) -trans-anti-B[a]P-N<sup>2</sup>-dG; NER, nucleotide excision repair; WMSA, water-mediated and substrate-assisted; MD, molecular dynamics; PDB, Protein Data Bank.

## REFERENCES

- (1) Hsu, G. W., Huang, X., Luneva, N. P., Geacintov, N. E., and Beese, L. S. (2005) Structure of a high fidelity DNA polymerase bound to a benzo[a]pyrene adduct that blocks replication. *J. Biol. Chem.* 280, 3764–3770.
- (2) Broyde, S., Wang, L., Rechkoblit, O., Geacintov, N. E., and Patel, D. J. (2008) Lesion processing: High-fidelity versus lesion-bypass DNA polymerases. *Trends Biochem. Sci.* 33, 209–219.
- (3) Yang, W. (2014) An Overview of Y-Family DNA Polymerases and a Case Study of Human DNA Polymerase  $\eta$ . *Biochemistry* 53, 2793–2803.
- (4) Friedberg, E. C., Lehmann, A. R., and Fuchs, R. P. (2005) Trading places: How do DNA polymerases switch during translesion DNA synthesis? *Mol. Cell* 18, 499–505.

- (5) Yang, W., and Woodgate, R. (2007) What a difference a decade makes: Insights into translesion DNA synthesis. *Proc. Natl. Acad. Sci. U.S.A.* **104**, 15591–15598.
- (6) McCulloch, S. D., and Kunkel, T. A. (2008) The fidelity of DNA synthesis by eukaryotic replicative and translesion synthesis polymerases. *Cell Res.* **18**, 148–161.
- (7) Sale, J. E., Lehmann, A. R., and Woodgate, R. (2012) Y-family DNA polymerases and their role in tolerance of cellular DNA damage. *Nat. Rev. Mol. Cell Biol.* **13**, 141–152.
- (8) Lone, S., Townson, S. A., Uljon, S. N., Johnson, R. E., Brahma, A., Nair, D. T., Prakash, S., Prakash, L., and Aggarwal, A. K. (2007) Human DNA polymerase  $\kappa$  encircles DNA: Implications for mismatch extension and lesion bypass. *Mol. Cell* **25**, 601–614.
- (9) Liu, Y., Yang, Y., Tang, T. S., Zhang, H., Wang, Z., Friedberg, E., Yang, W., and Guo, C. (2014) Variants of mouse DNA polymerase  $\kappa$  reveal a mechanism of efficient and accurate translesion synthesis past a benzo[a]pyrene dG adduct. *Proc. Natl. Acad. Sci. U.S.A.* **111**, 1789–1794.
- (10) Lior-Hoffmann, L., Wang, L., Wang, S., Geacintov, N. E., Broyde, S., and Zhang, Y. (2012) Preferred WMSA catalytic mechanism of the nucleotidyl transfer reaction in human DNA polymerase  $\kappa$  elucidates error-free bypass of a bulky DNA lesion. *Nucleic Acids Res.* **40**, 9193–9205.
- (11) Jia, L., Geacintov, N. E., and Broyde, S. (2008) The N-clasp of human DNA polymerase  $\kappa$  promotes blockage or error-free bypass of adenine- or guanine-benzo[a]pyrenyl lesions. *Nucleic Acids Res.* **36**, 6571–6584.
- (12) Zhang, Y., Yuan, F., Wu, X., Wang, M., Rechkoblit, O., Taylor, J. S., Geacintov, N. E., and Wang, Z. (2000) Error-free and error-prone lesion bypass by human DNA polymerase  $\kappa$  in vitro. *Nucleic Acids Res.* **28**, 4138–4146.
- (13) Choi, J. Y., Angel, K. C., and Guengerich, F. P. (2006) Translesion synthesis across bulky N2-alkyl guanine DNA adducts by human DNA polymerase  $\kappa$ . *J. Biol. Chem.* **281**, 21062–21072.
- (14) Poon, K., Itoh, S., Suzuki, N., Laxmi, Y. R., Yoshizawa, I., and Shibutani, S. (2008) Miscoding properties of 6 $\alpha$ - and 6 $\beta$ -diastereoisomers of the N(2)-(estradiol-6-yl)-2'-deoxyguanosine DNA adduct by Y-family human DNA polymerases. *Biochemistry* **47**, 6695–6701.
- (15) Yuan, B., Cao, H., Jiang, Y., Hong, H., and Wang, Y. (2008) Efficient and accurate bypass of N2-(1-carboxyethyl)-2'-deoxyguanosine by DinB DNA polymerase in vitro and in vivo. *Proc. Natl. Acad. Sci. U.S.A.* **105**, 8679–8684.
- (16) Zhang, Y., Wu, X., Guo, D., Rechkoblit, O., and Wang, Z. (2002) Activities of human DNA polymerase  $\kappa$  in response to the major benzo[a]pyrene DNA adduct: Error-free lesion bypass and extension synthesis from opposite the lesion. *DNA Repair* **1**, 559–569.
- (17) Rechkoblit, O., Zhang, Y., Guo, D., Wang, Z., Amin, S., Krzeminsky, J., Louneva, N., and Geacintov, N. E. (2002) trans-Lesion synthesis past bulky benzo[a]pyrene diol epoxide N<sup>2</sup>-dG and N<sup>6</sup>-dA lesions catalyzed by DNA bypass polymerases. *J. Biol. Chem.* **277**, 30488–30494.
- (18) Yasui, M., Dong, H., Bonala, R. R., Suzuki, N., Ohmori, H., Hanaoka, F., Johnson, F., Grollman, A. P., and Shibutani, S. (2004) Mutagenic properties of 3-(deoxyguanosin-N<sup>2</sup>-yl)-2-acetylaminofluorene, a persistent acetylaminofluorene-derived DNA adduct in mammalian cells. *Biochemistry* **43**, 15005–15013.
- (19) Song, I., Kim, E. J., Kim, I. H., Park, E. M., Lee, K. E., Shin, J. H., Guengerich, F. P., and Choi, J. Y. (2014) Biochemical Characterization of Eight Genetic Variants of Human DNA Polymerase  $\kappa$  Involved in Error-Free Bypass across Bulky N-Guanyl DNA Adducts. *Chem. Res. Toxicol.* **27**, 919–930.
- (20) Sassa, A., Niimi, N., Fujimoto, H., Katafuchi, A., Gruz, P., Yasui, M., Gupta, R. C., Johnson, F., Ohta, T., and Nohmi, T. (2011) Phenylalanine 171 is a molecular brake for translesion synthesis across benzo[a]pyrene-guanine adducts by human DNA polymerase  $\kappa$ . *Mutat. Res.* **718**, 10–17.
- (21) Suzuki, N., Ohashi, E., Hayashi, K., Ohmori, H., Grollman, A. P., and Shibutani, S. (2001) Translesional synthesis past acetylaminofluorene-derived DNA adducts catalyzed by human DNA polymerase  $\kappa$  and *Escherichia coli* DNA polymerase IV. *Biochemistry* **40**, 15176–15183.
- (22) Gerlach, V. L., Feaver, W. J., Fischhaber, P. L., and Friedberg, E. C. (2001) Purification and characterization of pol  $\kappa$ , a DNA polymerase encoded by the human DINB1 gene. *J. Biol. Chem.* **276**, 92–98.
- (23) Ohashi, E., Ogi, T., Kusumoto, R., Iwai, S., Masutani, C., Hanaoka, F., and Ohmori, H. (2000) Error-prone bypass of certain DNA lesions by the human DNA polymerase  $\kappa$ . *Genes Dev.* **14**, 1589–1594.
- (24) Sherrer, S. M., Sanman, L. E., Xia, C. X., Bolin, E. R., Malik, C. K., Efthimiopoulos, G., Basu, A. K., and Suo, Z. (2012) Kinetic analysis of the bypass of a bulky DNA lesion catalyzed by human Y-family DNA polymerases. *Chem. Res. Toxicol.* **25**, 730–740.
- (25) Sherrer, S. M., Taggart, D. J., Pack, L. R., Malik, C. K., Basu, A. K., and Suo, Z. (2012) Quantitative analysis of the mutagenic potential of 1-aminopyrene-DNA adduct bypass catalyzed by Y-family DNA polymerases. *Mutat. Res.* **737**, 25–33.
- (26) Kotapati, S., Maddukuri, L., Wickramaratne, S., Seneviratne, U., Goggin, M., Pence, M. G., Villalta, P., Guengerich, F. P., Marnett, L., and Tretyakova, N. (2012) Translesion synthesis across 1,N6-(2-hydroxy-3-hydroxymethylpropan-1,3-diy)-2'-deoxyadenosine (1,N6- $\gamma$ -HMHP-dA) adducts by human and archebacterial DNA polymerases. *J. Biol. Chem.* **287**, 38800–38811.
- (27) Liu, Y., Reeves, D., Kropachev, K., Cai, Y., Ding, S., Kolbanovskiy, M., Kolbanovskiy, A., Bolton, J. L., Broyde, S., Van Houten, B., and Geacintov, N. E. (2011) Probing for DNA damage with  $\beta$ -hairpins: Similarities in incision efficiencies of bulky DNA adducts by prokaryotic and human nucleotide excision repair systems in vitro. *DNA Repair* **10**, 684–696.
- (28) Geacintov, N. E., Cosman, M., Hingerty, B. E., Amin, S., Broyde, S., and Patel, D. J. (1997) NMR solution structures of stereoisomeric covalent polycyclic aromatic carcinogen-DNA adduct: Principles, patterns, and diversity. *Chem. Res. Toxicol.* **10**, 111–146.
- (29) Beije, B., and Möller, L. (1988) 2-Nitrofluorene and related compounds: Prevalence and biological effects. *Mutat. Res.* **196**, 177–209.
- (30) Beland, F. A., and Marques, M. M. (1994) DNA adducts of nitropolycyclic aromatic hydrocarbons. *IARC Sci. Publ.* **125**, 229–244.
- (31) Zaliznyak, T., Bonala, R., Johnson, F., and de Los Santos, C. (2006) Structure and stability of duplex DNA containing the 3-(deoxyguanosin-N2-yl)-2-acetylaminofluorene (dG(N2)-AAF) lesion: A bulky adduct that persists in cellular DNA. *Chem. Res. Toxicol.* **19**, 745–752.
- (32) Culp, S. J., Poirier, M. C., and Beland, F. A. (1993) Biphasic removal of DNA adducts in a repetitive DNA sequence after dietary administration of 2-acetylaminofluorene. *Environ. Health Perspect.* **99**, 273–275.
- (33) Cui, X. S., Eriksson, L. C., and Möller, L. (1999) Formation and persistence of DNA adducts during and after a long-term administration of 2-nitrofluorene. *Mutat. Res.* **442**, 9–18.
- (34) Westra, J. G., Kriek, E., and Hittenhausen, H. (1976) Identification of the persistently bound form of the carcinogen N-acetyl-2-aminofluorene to rat liver DNA in vivo. *Chem.-Biol. Interact.* **15**, 149–164.
- (35) Kropachev, K., Kolbanovskiy, M., Liu, Z., Cai, Y., Zhang, L., Schwaid, A. G., Kolbanovskiy, A., Ding, S., Amin, S., Broyde, S., and Geacintov, N. E. (2013) Adenine-DNA adducts derived from the highly tumorigenic dibenzo[a,l]pyrene are resistant to nucleotide excision repair while guanine adducts are not. *Chem. Res. Toxicol.* **26**, 783–793.
- (36) Hanawalt, P. C., and Spivak, G. (2008) Transcription-coupled DNA repair: Two decades of progress and surprises. *Nat. Rev. Mol. Cell Biol.* **9**, 958–970.
- (37) Spivak, G., and Ganesan, A. K. (2014) The complex choreography of transcription-coupled repair. *DNA Repair* **19**, 64–70.

- (38) Vermeulen, W., and Fousteri, M. (2013) Mammalian transcription-coupled excision repair. *Cold Spring Harbor Perspect. Biol.* 5, a012625.
- (39) Kitsera, N., Gasteiger, K., Luhnsdorf, B., Allgayer, J., Epe, B., Carell, T., and Khobta, A. (2014) Cockayne syndrome: Varied requirement of transcription-coupled nucleotide excision repair for the removal of three structurally different adducts from transcribed DNA. *PLoS One* 9, e94405.
- (40) Scharer, O. D. (2013) Nucleotide excision repair in eukaryotes. *Cold Spring Harbor Perspect. Biol.* 5, a012609.
- (41) Kisker, C., Kuper, J., and Van Houten, B. (2013) Prokaryotic nucleotide excision repair. *Cold Spring Harbor Perspect. Biol.* 5, a012591.
- (42) Berman, H. M., Battistuz, T., Bhat, T. N., Bluhm, W. F., Bourne, P. E., Burkhardt, K., Feng, Z., Gilliland, G. L., Iype, L., Jain, S., Fagan, P., Marvin, J., Padilla, D., Ravichandran, V., Schneider, B., Thanki, N., Weissig, H., Westbrook, J. D., and Zardecki, C. (2002) The Protein Data Bank. *Acta Crystallogr. D58*, 899–907.
- (43) Batra, V. K., Beard, W. A., Shock, D. D., Krahn, J. M., Pedersen, L. C., and Wilson, S. H. (2006) Magnesium-induced assembly of a complete DNA polymerase catalytic complex. *Structure* 14, 757–766.
- (44) Grad, R., Shapiro, R., Hingerty, B. E., and Broyde, S. (1997) A molecular mechanics and dynamics study of the minor adduct between DNA and the carcinogen 2-(acetylamino)fluorene (dG-N2-AAF). *Chem. Res. Toxicol.* 10, 1123–1132.
- (45) Case, D. A., Darden, T. A., Cheatham, T. E., III, Simmerling, C. L., Wang, J., Duke, R. E., Luo, R., Walker, R. C., Zhang, W., Merz, K. M., Roberts, B., Wang, B., Hayik, S., Roitberg, A., Seabra, G., Kolossaváry, I., Wong, K. F., Paesani, F., Vanicek, J., Liu, J., Wu, X., Brozell, S. R., Steinbrecher, T., Gohlke, H., Cai, Q., Ye, X., Wang, J., Hsieh, M.-J., Cui, G., Roe, D. R., Mathews, D. H., Seetin, M. G., Sagui, C., Babin, V., Luchko, T., Gusarov, S., Kovalenko, A., and Kollman, P. A. (2010) AMBER 11, University of California, San Francisco.
- (46) Cornell, W. D., Cieplak, P., Bayly, C. I., Gould, I. R., Merz, K. M., Ferguson, D. M., Spellmeyer, D. C., Fox, T., Caldwell, J. W., and Kollman, P. A. (1995) A second generation force field for the simulation of proteins, nucleic acids, and organic molecules. *J. Am. Chem. Soc.* 117, 5179–5197.
- (47) Wang, J. M., Cieplak, P., and Kollman, P. A. (2000) How well does a restrained electrostatic potential (RESP) model perform in calculating conformational energies of organic and biological molecules? *J. Comput. Chem.* 21, 1049–1074.
- (48) Perez, A., Marchan, I., Svozil, D., Sponer, J., Cheatham, T. E., III, Laughton, C. A., and Orozco, M. (2007) Refinement of the AMBER force field for nucleic acids: Improving the description of  $\alpha/\gamma$  conformers. *Biophys. J.* 92, 3817–3829.
- (49) Wang, J., Wolf, R. M., Caldwell, J. W., Kollman, P. A., and Case, D. A. (2004) Development and testing of a general Amber force field. *J. Comput. Chem.* 25, 1157–1174.
- (50) Price, D. J., and Brooks, C. L., III (2004) A modified TIP3P water potential for simulation with Ewald summation. *J. Chem. Phys.* 121, 10096–10103.
- (51) Perlow, R. A., and Broyde, S. (2002) Toward understanding the mutagenicity of an environmental carcinogen: Structural insights into nucleotide incorporation preferences. *J. Mol. Biol.* 322, 291–309.
- (52) Pymol. *The PyMOL Molecular Graphics System*, version 1.3, Schrödinger, LLC, Portland, OR.
- (53) Wang, L., Yu, X., Hu, P., Broyde, S., and Zhang, Y. (2007) A water-mediated and substrate-assisted catalytic mechanism for *Sulfolobus solfataricus* DNA polymerase IV. *J. Am. Chem. Soc.* 129, 4731–4737.
- (54) Steitz, T. A. (1998) A mechanism for all polymerases. *Nature* 391, 231–232.
- (55) Beard, W. A., and Wilson, S. H. (2014) Structure and Mechanism of DNA Polymerase  $\beta$ . *Biochemistry* 53, 2768–2780.
- (56) Nakamura, T., Zhao, Y., Yamagata, Y., Hua, Y. J., and Yang, W. (2012) Watching DNA polymerase  $\eta$  make a phosphodiester bond. *Nature* 487, 196–201.
- (57) Freudenthal, B. D., Beard, W. A., Shock, D. D., and Wilson, S. H. (2013) Observing a DNA polymerase choose right from wrong. *Cell* 154, 157–168.
- (58) Stancel, J. N., McDaniel, L. D., Velasco, S., Richardson, J., Guo, C., and Friedberg, E. C. (2009) Polk mutant mice have a spontaneous mutator phenotype. *DNA Repair* 8, 1355–1362.
- (59) Cosman, M., de los Santos, C., Fiala, R., Hingerty, B. E., Singh, S. B., Ibanez, V., Margulis, L. A., Live, D., Geacintov, N. E., Broyde, S., et al. (1992) Solution conformation of the major adduct between the carcinogen (+)-anti-benzo[a]pyrene diol epoxide and DNA. *Proc. Natl. Acad. Sci. U.S.A.* 89, 1914–1918.
- (60) Ogi, T., Shinkai, Y., Tanaka, K., and Ohmori, H. (2002) Polk protects mammalian cells against the lethal and mutagenic effects of benzo[a]pyrene. *Proc. Natl. Acad. Sci. U.S.A.* 99, 15548–15553.
- (61) Avkin, S., Goldsmith, M., Velasco-Miguel, S., Geacintov, N., Friedberg, E. C., and Livneh, Z. (2004) Quantitative analysis of translesion DNA synthesis across a benzo[a]pyrene-guanine adduct in mammalian cells: The role of DNA polymerase  $\kappa$ . *J. Biol. Chem.* 279, 53298–53305.
- (62) Bi, X., Slater, D. M., Ohmori, H., and Vaziri, C. (2005) DNA polymerase  $\kappa$  is specifically required for recovery from the benzo[a]pyrene-dihydrodiol epoxide (BPDE)-induced S-phase checkpoint. *J. Biol. Chem.* 280, 22343–22355.
- (63) Livneh, Z., Ziv, O., and Shachar, S. (2010) Multiple two-polymerase mechanisms in mammalian translesion DNA synthesis. *Cell Cycle* 9, 729–735.